NeuroImage 187 (2019) 116–127

Contents lists available at ScienceDirect

NeuroImage

journal homepage: www.elsevier.com/locate/neuroimage

BOLD signal physiology: Models and applications

C.J. Gauthier [a,*,1], A.P. Fan [b,1]

[a] Concordia University, Montreal, Canada
[b] Stanford University, California, USA

A B S T R A C T

The BOLD contrast mechanism has a complex relationship with functional brain activity, oxygen metabolism, and neurovascular factors. Accurate interpretation of the BOLD signal for neuroscience and clinical applications necessitates a clear understanding of the sources of BOLD contrast and its relationship to underlying physiology. This review describes the physiological components that contribute to the BOLD signal and the steady-state calibrated BOLD models that enable quantification of functional changes with a separate challenge paradigm. The principles derived from these biophysical models are then used to interpret BOLD measurements in different neurological disorders in the presence of confounding vascular factors related to disease.

BOLD contrast and physiology

The BOLD contrast in functional MRI results from the fact that oxygenated hemoglobin is diamagnetic, while deoxygenated hemoglobin (dHb) is paramagnetic. Because dHb is paramagnetic, water spins in partly deoxygenated blood experience increased dephasing. This dephasing attenuates the T2*-weighted signal from venous blood and tissue containing dHb (Ogawa et al., 1990a, 1990b). When the brain is performing a task, active regions consume oxygen to function, leading to a localized increase in dHb. To meet the need for additional oxygen, nearby blood vessels dilate, causing an increase in local blood flow. The inflowing blood is fully oxygenated, thereby diluting the dHb concentration and leading to an increased BOLD signal.

Because the activity-driven BOLD signal increase is due to vasodilation and dilution of dHb, the BOLD signal conflates changes in oxidative metabolism, blood flow and blood volume. This hemodynamic response is thought to be tightly regulated in healthy brains, but changes in neurovascular coupling in aging and disease make it problematic to compare BOLD signals across groups (Ances et al., 2008, 2009; Gauthier et al., 2013; Hutchison et al., 2013; Liu et al., 2013; Peng et al., 2014). These group comparisons are problematic both because of the physiological ambiguity of the BOLD signal and because BOLD contrast measures a relative signal change from an unknown baseline. Any change in coupling or in the baseline cerebral blood flow (CBF), cerebral blood volume (CBV) or oxygen metabolism will result in a different BOLD signal change. Therefore, the vascular and metabolic sub-components should be taken into account for the accurate interpretation of task-evoked and resting state BOLD signal changes (Liu, 2013).

Underlying neuronal activity

Functional imaging using hemodynamic methods such as BOLD contrast are based on the assumption that the signal changes observed are strongly correlated with underlying neuronal activity. Convincing evidence for this correlation comes from simultaneous electrophysiological and fMRI recordings in non-human primates (Logothetis et al., 2001; Logothetis and Wandell, 2004; Shmuel et al., 2002). In these studies, electrodes are inserted in monkey visual cortex to record spontaneous or visual task-elicited activity of neuronal currents simultaneously with fMRI signal in the same areas. Electrophysiological recordings capture three types of neuronal electrical activity: single unit spiking activity, multi-unit activity (MUA) and local field potentials (LFP). An electrode placed in the extracellular fluid measures MUA, which is thought to represent spiking activity from more distant neurons. LFP activity is thought to reflect predominantly sub-threshold currents in the soma and dendrites of surrounding neuron populations, with some contributions from voltage-gated membrane oscillations and membrane after-potentials (Logothetis and Wandell, 2004; Magri et al., 2012).

Early electrophysiological studies in anesthetized monkeys have established that while BOLD signal amplitude is correlated with all types of neuronal firing, it is more closely linked with local field potentials (LFPs) than with other electrical activity such as spikes from action potentials (Logothetis et al., 2001). While higher frequency bands such as gamma (40–100 Hz) were the most informative about the BOLD signal, the relative power distribution across the bands carries complementary information (Magri et al., 2012). For instance, BOLD signal increases correlate with a shift in the power of LFPs towards higher frequencies

* Corresponding author. Department of Physics, Concordia University, Montreal, Canada.
E-mail address: claudine.gauthier@concordia.ca (C.J. Gauthier).
[1] Authors contributed equally to the manuscript.

https://doi.org/10.1016/j.neuroimage.2018.03.018
Received 16 November 2017; Received in revised form 14 February 2018; Accepted 8 March 2018
Available online 13 March 2018

(Magri et al., 2012), in agreement with theory (Kilner et al., 2005). These relationships were found to be true also for BOLD signal decreases, with shifts towards lower frequencies indicative of a deactivation (Magri et al., 2012). However, studies have shown that there may be non-linearities in the relationship between stimuli amplitude and type, neuronal response and hemodynamic signals (Bartolo et al., 2011; Bentley et al., 2016; Devor et al., 2003). Taken together, these results illustrate a complex relationship between neuronal activity and the BOLD signal, such that a simple interpretation of BOLD signal in terms of activation should be considered cautiously.

Oxidative metabolism

While the BOLD signal is related to electrical activity, the signal itself arises from a combination of changes in blood flow, blood volume and oxidative metabolism to meet the energy demands of brain activity. Therefore, the contribution of oxidative metabolism versus aerobic glycolysis to brain energy expenditure linked to neuronal activity is an important consideration to understand the relationship between the BOLD signal and neuronal activity.

The main energy expenditure of neurons is to maintain membrane potential in preparation to fire action potentials and integrate synaptic information when the need arises. To do so, the brain uses energy in the form of ATP, which is derived from the metabolism of glucose. Two forms of glucose metabolism in the presence of oxygen exist: aerobic glycolysis, which is faster but only produces 2 ATP molecules per glucose; and oxidative phosphorylation through the mitochondrial electron transport chain, which is highly efficient, forming as many as 38 ATP molecules from a single glucose molecule. Because oxidative phosphorylation is much more efficient at energy production and because the brain is known to be an avid user of oxygen, it was expected that oxidative metabolism would be the main form of metabolism used in the brain. Indeed, interruption of the brain's oxygen supply leads to unconsciousness within seconds and irreversible tissue damage within minutes as shown in a rat model (Levy et al., 1975). While initial Positron Emission Tomography (PET) results were consistent with a predominant role of aerobic glycolysis (Fox and Raichle, 1986), subsequent PET experiments have yielded results much more compatible with the predicted predominant role of oxidative metabolism (Hattori et al., 2004; Hyder et al., 2016; Ibaraki et al., 2008, 2010; Ishii et al., 1996b; Ito et al., 2005; Mintun et al., 2002; Yamauchi et al., 2002). Brain ATP generation is now thought to occur primarily through oxidative phosphorylation.

Neurovascular coupling

Because the brain has no stores of oxygen and glucose, brain tissue must meet increased metabolic demands during functional activity through local CBF increases, to deliver metabolic substrates and remove waste. The neurovascular unit is composed of different cells which work together to orchestrate the blood flow increase required by increased metabolic demand. The neurovascular unit includes neurons, glia and vascular cells, including vessel endothelium, smooth muscle cells, pericytes and adventitial cells (Girouard and Iadecola, 2006). The signalling cascades that underlie this process of neurovascular coupling are complex and may be regionally dependent (Lecrux and Hamel, 2016). While research in this area has identified the main mediators and modulators of this pathway (Girouard and Iadecola, 2006; Lauritzen and Gold, 2003; Lecrux and Hamel, 2011, 2016), their relative importance and the cellular environment variables that determine their function are still largely unknown.

The regulation of blood flow via neurovascular coupling is complex and the amplitude of the hemodynamic response may depend strongly on the specific cellular environment of brain regions (Lecrux and Hamel, 2016). However, in all cases, there is some relationship between aspects of neuronal signalling and the release of vasoactive molecules. Therefore, though the exact underpinning of this blood flow response may be difficult to untangle, the response itself can be taken as a surrogate for neuronal activity. Much of our understanding about the spatial localization of neurovascular coupling and which blood compartments are altered during neural activity (and at what time) come from high-resolution, invasive optical imaging observations in rodent models (Berwick et al., 2005; Briers, 2001; Devor et al., 2003).

During performance of a task, the coupling ratio between the increase in blood flow to the increase in oxidative metabolism is thought to be around two under normal circumstances (Buxton, 2010). In other words, during local brain activity in the absence of disease or pharmacological agents, the fractional blood flow change is thought to be about two times larger than the fractional change in oxidative metabolism (Buxton, 2010; Leontiev et al., 2013). This fraction may however depend on the task, and may be changed in caffeine intake and disease, as well as across brain areas (Ances et al., 2011; Perthen et al., 2008).

Cerebral blood volume

Robust increases to cerebral blood volume (CBV), the volume of blood within a brain region, occur during functional activation and are known to modulate the BOLD signal (Toronov et al., 2003). Since CBV changes are strongly correlated with changes in CBF, the relationship between the BOLD signal and CBV is typically inferred from observed changes in perfusion. This power law relationship is described by $CBV \sim CBF^{\alpha}$, where α is the Grubb constant and has reported values in the range of 0.38–0.50 (Eichling et al., 1975; Malonek et al., 1997; van Zijl et al., 1998) in animal models (rhesus monkeys, rodents) and healthy persons. However, it is likely that the temporal evolution of CBF and CBV are not matched throughout the BOLD time course, potentially creating transient effects such as the initial dip and post-stimulus undershoot (Mandeville et al., 1999; van Zijl et al., 2012). Furthermore, the CBF-CBV coupling likely changes during gas breathing or pharmacological agents (Seifritz et al., 2000), and is known to be disrupted in neurological disorders such as tumours and carotid stenosis. In these scenarios, a direct, quantitative measurement of CBV would inform the BOLD model independently of perfusion measurements.

Direct CBV measurement has been shown to be functionally sensitive across many parenchymal brain structures (Mandeville et al., 1999); and to localize to deep cortical layers (Jin and Kim, 2008). Thus, CBV as a way to map brain activity offers improved spatial localization than gradient-echo BOLD signal (Aaslid et al., 1984; Kim et al., 2013), which is prone to contamination by signal from remote large veins. Highly sensitive sequences with MRI contrast agent (Francis et al., 2003) and without contrast (Donahue et al., 2006; Huber et al., 2018; Lu and van Zijl, 2012) have been developed for high-resolution observation of CBV. Furthermore, localization of CBV in specific vascular compartments would also be useful for interpretation of BOLD contrast. While the BOLD response is thought to be mostly affected by changes in venous blood volume (CBV_v) (Buxton et al., 1998) most imaging methods measure total CBV as a proxy for CBV_v. Recent hypercapnia studies in rat models reported a substantial arterial component (~36%) to total blood volume change (Lee et al., 2001). If this arterial contribution is neglected, the estimated response in oxidative metabolism for a given BOLD signal will be underestimated. New independent quantification methods (Stefanovic and Pike, 2005) that specifically target venous CBV would help understand the mechanism of BOLD fMRI.

BOLD signal models

Given the complex and ambiguous nature of the BOLD signal, an accurate model of the vascular and metabolic contributions to signal would be useful to better understand differences across brain regions and groups. Over the years, there are two categories of models that have evolved: some focus on the dynamic aspects of the BOLD signal such as the BOLD signal time course and the post-stimulus undershoot; while others attempt to separate the steady-state physiological components,

e.g. with respiratory calibrations. This review will address dynamic models only superficially and focus on the steady-state models, although we refer the reader to other reviews on dynamic models (Buxton, 2010, 2012). The theory for calibrated fMRI has previously been reviewed (Blockley et al., 2013; Pike, 2012), but here we describe recent, advanced methods for baseline oxygenation with calibrated BOLD models and later describe considerations for its use in disease.

Dynamic models of the BOLD signal

One family of dynamic models for the BOLD time course has followed the original formulation by Buxton et al. of the so-called balloon model (Buxton et al., 1998). This model stems from the principles that (1) CBF increases more than $CMRO_2$ during the hemodynamic response to prevent a fall in tissue pO_2; and that (2) while the diameter of arteries is tightly controlled, the diameter of veins is purely a passive reflection of flow pressure. A review of this class of modeling can be found in (Buxton, 2012). A similar biophysical model was developed by Mandeville et al. to explain the underlying physiology responsible for delayed vascular compliance, which recreates the BOLD signal undershoot (Mandeville et al., 1999).

Expansions of these models have been informed by a more complex picture of the hemodynamic process (Aubert and Costalat, 2002; Aubert et al., 2007; Blockley et al., 2009; Buxton et al., 2004; Feng et al., 2001; Kong et al., 2004; Toronov et al., 2003; Uludag et al., 2009; Zheng and Mayhew, 2009). For example, newer dynamic models proposed by Havlicek et al. incorporate feed-forward neurovascular coupling that connects neural activity to blood flow, a balloon model that accommodates vascular uncoupling between CBF and CBV (Havlicek et al., 2015), and can synthesize BOLD data with CBF data collected concurrently during the same functional task (Havlicek et al., 2017b). Evidence that $CMRO_2$ may be elevated after the end of a stimulus (Donahue et al., 2009; Hua et al., 2011) suggests an alternative reason for the BOLD signal undershoot; but remains a topic of current debate as other studies indicate that CBF-CBV uncoupling causes the undershoot (Chen and Pike, 2009b, 2010; Havlicek et al., 2017a). Further evidence that tissue pO_2 is not as close to 0 as originally postulated (Devor et al., 2011) has also led to sophisticated modifications of BOLD dynamic models. These models and advanced bottom-up biophysical models (Gagnon et al., 2015) are valuable to predict the BOLD signal and validate existing physiological interpretations of the signal.

Calibrated fMRI models

Calibrated fMRI is a family of techniques used to estimate oxidative metabolism in the brain, using a combination of a steady-state BOLD biophysical model and a respiratory manipulation. While this formulation was originally developed as a biophysical model of the BOLD signal, a more recent understanding of the complexity of neurovascular coupling has led calibrated fMRI to be viewed as a useful heuristic simplification (Buxton, 2012; Gagnon et al., 2016; Griffeth and Buxton, 2011). Calibrated fMRI enables experimental measurement of the BOLD signal sub-components and metabolism, and its predictions are in good agreement with more complex biophysical models (Griffeth and Buxton, 2011), especially when the assumed parameters are used as heuristic constants (Gagnon et al., 2016; Griffeth and Buxton, 2011).

The original calibrated fMRI models allowed the measurement of task-evoked changes in cerebral metabolic rate of O_2 consumption ($CMRO_2$). Recent developments have however focused on measurement of resting $CMRO_2$. Measurement of task-evoked oxidative metabolism provides quantitative estimates of $CMRO_2$ which can help us understand functional differences across groups even if they have different vascular properties, such as older compared to younger adults (Ances et al., 2009; Gauthier et al., 2013; Mohtasib et al., 2012) or in certain diseases such as dementia and HIV (Ances et al., 2011). As a quantitative approach, baseline oxidative metabolism mapping may be more powerful as a potential biomarker in diseases with altered oxygen extraction fraction (OEF), including stroke, carotid occlusion, aging, dementia and other cerebrovascular diseases (Aanerud et al., 2012; De Vis et al., 2015a, 2015b; Ishii et al., 1996a; Lu et al., 2011; Yamauchi et al., 2009).

Hypercapnia model

In the calibrated fMRI model proposed by Davis et al. (1998) and described by Hoge et al. (1999), a hypercapnia manipulation is used to evoke a putatively purely vascular BOLD signal change. One of the main assumptions of this model is that breathing moderate CO_2 concentrations on the order of 5% causes vasodilation and increases blood flow without changing oxidative metabolism. During the hypercapnia challenge, a dual echo sequence is typically used to measure CBF with ASL (at a short echo) and BOLD contrast at a longer echo (~30 ms at 3 T) that optimizes sensitivity to the BOLD signal. The CBF and BOLD measurements are used as inputs into the hypercapnia model model (Davis et al., 1998; Hoge et al., 1999) to estimate M, a calibration parameter. M corresponds to the maximum possible BOLD signal change and is equivalent to the BOLD signal one would measure if all the dHb present at baseline were removed from the voxel. The hypercapnia model relates these quantities as follows:

$$M = \frac{\frac{\Delta BOLD}{BOLD}}{\frac{1-CBF^{-(\beta-\alpha)}}{CBE_0}} \quad (1)$$

There are four assumed parameters in the hypercapnia model. Alpha represents the CBF to CBV coupling ratio, which was typically assumed to be uniform throughout the brain and across individuals. More recent studies have directly measured the exponent relating CBV and CBF in humans, e.g. with VERVE MRI to focus on venous instead of total blood volume (Chen and Pike, 2009a, 2010). The value for the alpha parameter is now thought to be around 0.18–0.20, lower than in the original experiment by Grubb et al. (0.38). Beta represents the field-dependent influence of dHb on transverse relaxation (Boxerman et al., 1995) and is assumed to be 1.3–1.5 at 3T (Bulte et al., 2009; Gauthier et al., 2013; Hare et al., 2015). More recent approaches treat Equation (1) as a heuristic model and estimate alpha and beta as heuristics constants without a specific physiological interpretations (Gagnon et al., 2016; Griffeth and Buxton, 2011). In these heuristic models, alpha and beta are found to have lower values than their original biophysical values.

A third assumed parameter is that arterial blood is fully oxygen saturated, and arterial oxygen saturation tends to be >97% in healthy adults even in slightly hypoxic conditions (Lu et al., 2012). However, measurements of oxygen tension have recently suggested that a relatively large amount of oxygen exits in pial arterioles prior to reaching the capillary bed (Vazquez et al., 2010), and assuming arterial O_2 saturation may be problematic in disease populations (Bernardi et al., 2017; Ogburn-Russell and Johnson, 1990; Vold et al., 2014). Finally, the assumption of iso-metabolism during the hypercapnia manipulation may be somewhat problematic as there are indications that even moderate CO_2 concentration may suppress oxidative metabolism (Xu et al., 2011b; Zappe et al., 2008).

The hypercapnia model also describes the relationship between M and $CMRO_2$ evoked during a task. This is calculated using M (from hypercapnia), alpha and beta (which have the same values as before), and the BOLD and CBF responses during a functional task:

$$\frac{CMRO_2}{CMRO_{20}} = \frac{CBF^{1-\alpha/\beta}}{CBF_0}\left(1 - \frac{\frac{\Delta BOLD}{BOLD_0}}{M}\right)^{1/\beta} \quad (2)$$

All subsequent versions of the model use this equation to relate M to task-evoked BOLD signal, ASL and $CMRO_2$.

Hyperoxia model

Because even moderate concentrations of CO_2 can cause dyspnea and discomfort, a related model was developed using hyperoxia instead of

hypercapnia for calibration. The hyperoxia method (Chiarelli et al., 2007) also assumes that the breathing manipulation does not affect the rate of oxidative metabolism. This assumption is also debated and there are indications that while elevated O_2 concentrations may not be perceptible, they may nevertheless impact oxidative metabolism (Xu et al., 2011a). One of the main differences of the hyperoxia model is how it takes into account CBF to derive an estimate of M. Elevated inspired O_2 concentrations do not have a large effect on CBF, so the CBF change is usually assumed in this technique. Relatively low O_2 concentrations are typically used to avoid significant vasoconstriction (Chiarelli et al., 2007; Mark et al., 2011) and the decreased CBF that may occur in fixed-inspired hyperoxia manipulations (Fan et al., 2016; Gauthier and Hoge, 2012a). Therefore, in most implementations, the CBF change is assumed to be 0. In the hyperoxia model, M is calculated using the BOLD signal, an assumed CBF change, expired O_2 concentrations, and assumed constants. The assumed constants are baseline oxygen extraction fraction (OEF), used to calculate the venous dHb concentration, as well as the same alpha and beta constants present in the hypercapnia model.

$$\frac{\Delta BOLD}{BOLD} = M\left(1 - \left(\frac{CBF}{CBF_0}\right)^{a}\left(\frac{[dHb]_v}{[dHb]_{v0}} + \frac{CBF_0}{CBF} - 1\right)^{\beta}\right) \quad (3)$$

The hyperoxia technique has been used to study aging-related cognitive changes (Mohtasib et al., 2012). This model has been shown to have a reduced measurement variance compared to the hypercapnia technique (Gauthier and Hoge, 2012a; Mark et al., 2011). This lower variability is due to the fact that flow changes are assumed rather than measured when calculating M. There are, however, indications that this assumption leads to systematic underestimation of the M parameter and thus underestimation of the $CMRO_2$ change during a task (Gauthier and Hoge, 2012a).

Generalized calibration model

Following the development of the hyperoxia model, modifications to generalize this approach for both hypercapnia and hyperoxia led to formulation of the generalized calibration model (GCM) (Gauthier and Hoge, 2012a). The GCM model extends the hyperoxia calibration model to include CBF in the equation relating the arterial and venous concentrations of O_2:

$$Cv_{O_2} = Ca_{O_2} - \frac{\left(Ca_{O_2}|_0 . OEF_0\right)}{\left(\frac{CBF}{CBF_0}\right)} \quad (4)$$

This modification allows the GCM model to be used any arbitrary combination of changes in O_2 and CO_2. Because both CBF and expired O_2 concentrations are used to calculate M, estimates of M obtained using the GCM have been shown to be more stable (Gauthier and Hoge, 2012a) and more similar to directly measured M values (Gauthier et al., 2011) than the hypercapnia and hyperoxia models.

Baseline $CMRO_2$ mapping with respiratory calibration and BOLD signal

Baseline oxidative metabolism has been shown by PET to be affected in several diseases, but there is no gold standard to non-invasively measure regional $CMRO_2$ with MRI. The most established imaging technique is triple ^{15}O-PET, which uses ^{15}O-labelled H_2O, O_2 and CO to measure OEF, CBF and $CMRO_2$ (Ishii et al., 1996a, 1996b; Ito et al., 2004; Yamaguchi et al., 1986). PET studies using this technique have shown metabolic changes in stroke (Yamaguchi et al., 1986), dementia (Nagata et al., 2000) and Alzheimer's disease (Ishii et al., 1996b). Unfortunately, ^{15}O-radiotracers have a half life of 2 min, so PET measurement of oxidative metabolism requires specialized equipment, complex setup, and invasive arterial blood sampling for quantification. These constraints make ^{15}O-PET difficult to implement in clinical settings and in most research institutes.

In recent years, MRI techniques have been developed to measure baseline OEF and $CMRO_2$ from calibrated BOLD. In the original hyperoxia and GCM biophysical models, the value of the resting OEF is explicitly assumed. Instead of assuming baseline OEF, several groups have modified the BOLD model to measure OEF through use of multiple respiratory calibrations. This would allow calibrated fMRI to be used not only for mapping task-evoked metabolism, but also baseline metabolism (Bulte et al., 2012; Gauthier and Hoge, 2012b; Wise et al., 2013).

The dual-calibration method proposed by Bulte et al. (2012) uses two breathing manipulations (hypercapnia and hyperoxia) and simultaneously measures BOLD signal, ASL and end-tidal O_2 values (Fig. 1a,b). The BOLD and ASL signals during the hypercapnia manipulation are first used to measure M with the hypercapnia model (Davis et al., 1998). This M value is then combined with BOLD and end-tidal O_2 measurements from a separate hyperoxia manipulation to estimate baseline OEF, instead of assuming OEF as in the original hyperoxia model (Chiarelli et al., 2007). OEF can then be combined with resting CBF from a baseline ASL measurement to estimate resting $CMRO_2$ through the Fick principle (Kety and Schmidt, 1948). This approach relies on two sets of assumptions (from the hypercapnia and hyperoxia models) to measure M and OEF, and has been used to study aging and carotid occlusion (De Vis et al., 2015a, 2015b).

Gauthier and Hoge proposed an alternative approach to map baseline $CMRO_2$ based on the GCM, which uses two or more breathing manipulations to measure OEF and M simultaneously (Gauthier and Hoge, 2012b) (Fig. 1c). The GCM can be expressed as the relationship between measured quantities (BOLD signal, ASL and end-tidal O_2), with two unknown parameters (M and OEF). This equation can be adapted for any breathing manipulation with changes in CO_2, O_2 or both. Therefore, by performing two or more breathing challenges, both unknowns OEF and M can be estimated. Because the measurements rely on a non-linear combination of low-SNR measurements such as ASL, three gases are sometimes used to increase the reliability of estimates (Fan et al., 2016; Gauthier et al., 2012; Gauthier and Hoge, 2012b).

A similar generalized, calibrated fMRI approach was subsequently proposed by Wise et al. (Wise et al., 2013) to simultaneously measure M, OEF and $CMRO_2$ using more complex hypercapnic and hyperoxic manipulations. These breathing manipulations combine several levels of O_2 and CO_2 inhalations to provide a more complete picture of the relationship between BOLD signal, CBF, and end-tidal O_2, with OEF and $CMRO_2$. It furthermore allows estimation of the α and β parameters or a heuristic combination of the two (Merola et al., 2016). This generalized model has also been implemented in a Bayesian statistical framework to improve reliability in low-SNR conditions, yielding promising and stable estimates of M, OEF and $CMRO_2$ (Germuska et al., 2016).

Potential sources of error as well as the reproducibility of baseline oxygenation mapping with calibrated BOLD models have been explored (Fan et al., 2016; Lajoie et al., 2016; Leontiev and Buxton, 2007). Technical considerations of the dual-calibration approach and their impact on estimates of metabolism were simulated by Blockley et al. (2015). The most problematic assumptions identified in healthy volunteers were the assumption of iso-metabolism under hypercapnia and the assumption of a small or non-existent CBF change during hyperoxia. Small deviations in these assumptions were found to lead to significant errors in OEF estimates. A recent 7 T MRI study observed 8% variation in $CMRO_2$ between adjacent scans and 33% variation across days (Krieger et al., 2014). In practice, quantification from calibrated BOLD models will depend on field strength. For instance, BOLD signals at higher magnetic fields (e.g, 7T) are more sensitive to microvasculature instead of larger veins, which corresponds to a smaller beta parameter ($\beta \sim 1$) in the model. The BOLD contribution also disproportionately decreases the sensitivity of ASL at higher field strengths, which propagates error into $CMRO_2$ estimates (Lu et al., 2006). Nonetheless, BOLD calibrations such as hypercapnia have been shown to provide consistent normalizations across field strengths and pulse sequences, suggesting that use of multiple respiratory calibrations may mitigate variations due to field strength (Cohen et al., 2004).

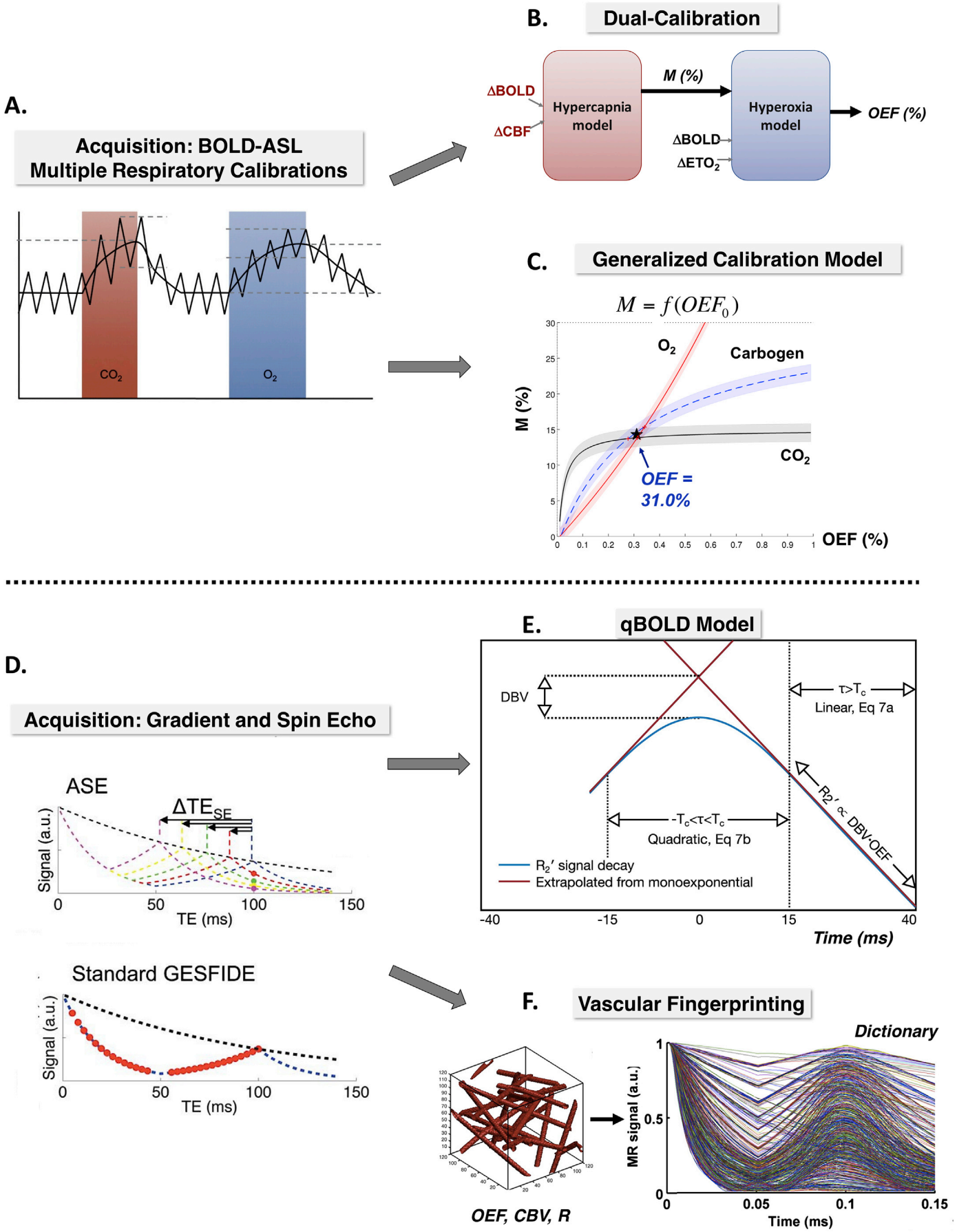

(caption on next page)

Fig. 1. Methods to quantify oxygenation from the BOLD signal. (A) Respiratory calibration approaches acquire BOLD signal, ASL (perfusion), and end-tidal gas measurements during multiple gas challenges, including hyperoxia, hypercapnia, and/or carbogen. (B) The analysis is performed with a dual-calibration approach, which first estimates the M parameter (maximum achievable BOLD) signal from the hypercapnia scan and then estimates baseline OEF from the hyperoxia scan (Bulte et al., 2012). (C) Alternatively, the generalized calibration model describes relationships between M and baseline OEF for any combination of gases, and estimates OEF from the curve intercept (Gauthier and Hoge, 2012b). (D) Independently, quantitative BOLD approaches acquire spin- and gradient-echo sampling of the BOLD signal. These sequences include asymmetric spin echo (ASE) and GESFIDE (gradient-echo sampling of free induction decay and echo) (Ni et al., 2015). (E) The multi-echo time course can then be fit to the quantitative BOLD model, which includes considers both OEF and deoxygenated blood volume (DBV) effects on the signal (Stone and Blockley, 2017). (F) In a fingerprinting approach, the signal time course can instead be matched to a best-fit curve in a simulated dictionary (Christen et al., 2014). This best-fit vascular fingerprint reveals the underlying OEF, vessel radius, and CBV of the voxel.

Baseline oxygenation mapping by quantitative BOLD (qBOLD) and vascular fingerprinting

Independent quantitative BOLD (qBOLD) approaches have been developed to model the BOLD magnitude signal and relaxation times (T2*, T2, T2′) in tissue and map baseline oxygenation without calibration. These relaxation times are modulated by local field inhomogeneities created by dHb molecules in microvasculature, and are thus sensitive to oxygenation levels. The T2′ parameter, which is the reversible component of transverse relaxation and defined as $1/T2' = 1/T2^* - 1/T2$, is the most directly related to oxygenation (Yablonskiy and Haacke, 1994). New hybrid sequences combine gradient and spin echo (multi-echo) acquisitions allow estimation of T2*, T2, and T2′ from the same scan (Ni et al., 2015; Yablonskiy and Haacke, 1997). These hybrid sequences enable mapping of relaxation parameters that are sensitive to the underlying oxygenation state of the brain. The GESFIDE (gradient-echo sampling of free induction decay and echo) sequence provides more repeatable R2' measurements compared to the original asymmetric spin echo sequence (Fig. 1d) (Ni et al., 2015).

A major challenge of extravascular BOLD methods is that relaxation parameters are not specific to brain oxygenation. For instance, even T2′ is the product of deoxygenated blood volume (DBV) and dHb-induced frequency shifts, and complex biophysical models are required to extract baseline oxygenation. Early quantitative BOLD (qBOLD) approaches have focused on the T2' signal from gradient- and spin-echo acquisitions. These methods model capillary vessels in brain parenchyma as a network of randomly oriented cylinders to describe MRI signal dephasing in the presence of dHb:

$$R2' = DBV \cdot \delta\omega = DBV \cdot \gamma \cdot 4/3 \cdot \pi \Delta\chi_0 \cdot 0.03\,[dHb]\,B_0 \quad (5)$$

where $\delta\omega$ is the characteristic frequency, γ is the gyromagnetic ratio, $\Delta\chi_0$ is the susceptibility difference between fully oxygenated and fully deoxygenated red blood cells, [dHb] is the hemoglobin concentration, and B_0 is the field strength. By fitting the signal model at each voxel, qBOLD techniques create parametric maps of venous oxygen saturation (SvO_2) and $CMRO_2$. Some qBOLD implementations assume a single extravascular tissue compartment (An and Lin, 2000; An et al., 2001), while others also consider blood and cerebrospinal fluid (CSF) compartments in the model fit to each voxel (Christen et al., 2012; He and Yablonskiy, 2007; He et al., 2008). Recent streamlined approaches consider the monoexponential and quadratic behaviors of transverse MR signal decay to separate OEF from blood volume effects on BOLD signal (Fig. 1e) (Stone and Blockley, 2017). The accuracy of qBOLD models also benefit from prospective correction for macroscopic field inhomogeneities (Blockley and Stone, 2016) and FLAIR suppression of CSF signal as confounders.

A novel extension of the qBOLD class of methods is vascular fingerprinting. Christen et al. proposed a vascular fingerprint that simulates a dictionary of signal curves based on gradient- and spin-echo acquisition (Fig. 1f). Each dictionary entry corresponds to the signal that would arise for specific combination of cerebral blood volume, mean vessel radius, and SvO_2 of microvasculature in a voxel (Christen et al., 2014). The actual measured signal is matched to the best-fit dictionary curve, which reveals a specific quantitative SvO_2 value (and other physiology) for tissue in the voxel. Design of efficient and orthogonal fingerprints (BOLD acquisition patterns) and use of realistic vessel models (e.g. from high-resolution optical microscopy (Pouliot et al., 2017)) will improve vascular fingerprinting approaches.

Future directions for oxygenation measurement from BOLD signal should also include validation with other modalities (PET and NIRS) and with alternative MRI methods. These MRI methods use different contrast mechanisms from BOLD, including T2 measurements in isolated venous blood (Bolar et al., 2011; Lu and Ge, 2008) and phase/susceptibility measurements in individual cerebral veins (Fan et al., 2011; Jain et al., 2010) or parenchyma (Zhang et al., 2016). These distinct oxygenation MRI methods have been reviewed in detail (Christen et al., 2013; Rodgers et al., 2016; Wehrli et al., 2016) and like quantitative BOLD models have nascent neuroscience and disease applications.

BOLD signal quantification in neurological disease

As described in the biophysical models above, extensive neuroscience investigations have sought to model and predict the BOLD signal from its quantitative components, including blood flow, blood volume, and blood oxygenation (Cheng and Haacke, 2001; van Zijl et al., 1998). However, these models have focused on normal physiology in functional activity, and are challenging to apply in disease settings. In various neurological disorders, pathological processes will perturb multiple physiological parameters, which are difficult to disentangle from a single BOLD measurement.

In tumours, for instance, BOLD MRI has been proposed as a proxy biomarker for tissue oxygenation, especially during interventions that seek to enhance the radiation response of poorly oxygenated tumours (Dunn et al., 2002). Unfortunately, the BOLD signal alone cannot be used to assess absolute oxygenation. Previous studies in mice models found no correlation between BOLD signal and direct pO_2 measurement (with micro-optic probes) across tumours (Baudelet and Gallez, 2002); e.g. a given BOLD signal change could correspond to 25 mmHg pO_2 change in one tumour but to 100 mmHg pO_2 change in another tumour. Similarly, baseline pO_2 did not relate to the baseline T2* (BOLD-weighted) signal. Interpreting BOLD contrast as a biomarker of oxygenation is thus an over-simplification, likely because it neglects the flow weighting in the signal.

Cerebrovascular reactivity

On the other hand, fluctuations in BOLD signal do correlate over time with pO_2 changes (Hallac et al., 2014), suggesting that BOLD responses to manipulations (such as carbogen breathing) can inform scientists and clinicians about the physiological response in individual tumours (Taylor et al., 2001). Monitoring the hemodynamic response to different gas challenges, such as a hyperoxia and hypercapnia, may allow discrimination between tumours and healthy tissue, and between different tumour types (Ben Bashat et al., 2012). In fact, a negative BOLD response during hypercapnia (which increases blood flow globally to the brain) has been observed in tissue distal to the tumour location (Ben Bashat et al., 2012). This negative response is indicative of steal phenomenon, in which blood flow is shunted away from ischemic areas that lack auto-regulation of flow. In this case, the BOLD signal change is dominated by the flow response instead of its sensitivity to oxygenation.

These observations in tumours are echoed by findings in

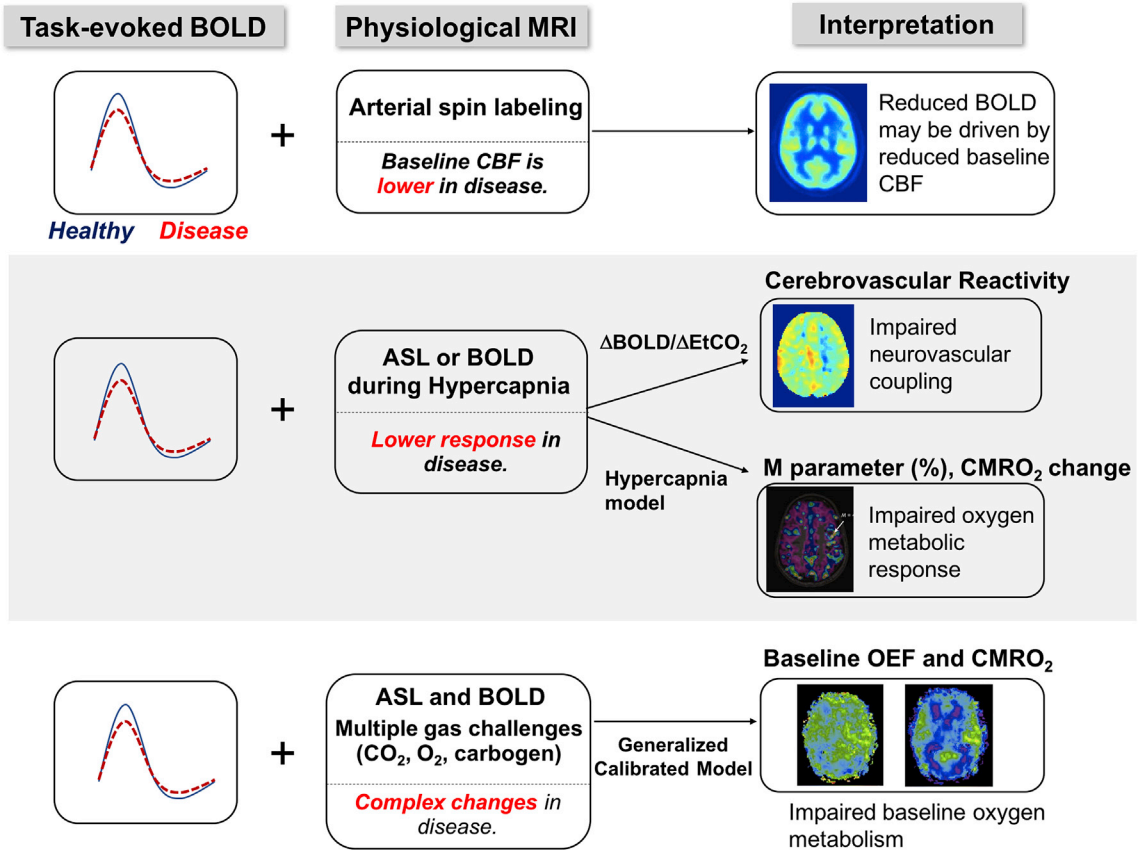

Fig. 2. BOLD quantification in disease. Disease-related changes to the BOLD signal amplitude may be driven by differences in neuronal activity or by vascular differences between patients (red) and healthy controls (blue). With an additional arterial spin labeling (ASL) MRI scan, baseline CBF can be measured in the same imaging session. Reduced perfusion in some patients accounts for lower BOLD signal, including in several neurodegenerative diseases and cognitive aging. With a single hypercapnia challenge, the change in BOLD or ASL signal during gas breathing reveals the cerebrovascular reactivity of brain tissue. If both BOLD and ASL contrasts are acquired during hypercapnia, quantitative modeling reveals the M parameter (maximum achievable BOLD signal) and task-driven change in cerebral metabolic rate of oxygen ($CMRO_2$). Physiological MRI during hypercapnia thus assesses whether neurovascular coupling and the oxygen metabolic response is preserved or impaired in patients, which would reduce the BOLD signal. Finally, with multiple respiratory calibrations, quantitative maps of baseline oxygen extraction fraction (OEF) and $CMRO_2$ are available to control the BOLD signal for oxygen metabolism or compare physiology directly between groups.

cerebrovascular disease; BOLD increases during gas breathing or during a pharmacological (acetazolamide) challenge in steno-occlusive patients strongly correlate with quantitative perfusion changes (De Vis et al., 2015b; Mandell et al., 2008). Comparing the cerebrovascular reactivity (CVR) in response to a "stress challenge" between patient groups is more appropriate than a direct comparison of baseline BOLD signal, and can help interpret separate BOLD observations during a functional task. For instance, "normal-appearing" tissue areas in patients with stroke were found to have the same CVR as control subjects (Geranmayeh et al., 2015). In these normal-appearing regions, any group-level BOLD signal changes during a functional task is likely neuronal in nature, if baseline CBF is also unaffected.

In the same stroke patients, CVR was reduced in tissue near the infarct, but this CVR level was maintained throughout multiple repeated sessions. As CVR measurements were repeatable, longitudinal group-level BOLD changes during the functional task were confidently attributed to neuronal changes in the stroke patients (e.g. recovery over time) instead of vascular changes (Geranmayeh et al., 2015). On the other hand, large BOLD CVR differences have been measured between APOE ε2-and ε4-gene carriers, who are at higher risk of Alzheimer's dementia, versus non-carriers. These genotype differences in CVR accounted for 70% of hippocampal BOLD differences between groups during a functional memory task (Suri et al., 2014), suggesting that a task-evoked BOLD experiment alone cannot capture APOE's effect (likely vascular) on risk for Alzheimer's disease.

BOLD contrast combined with physiological imaging

The most informative patient studies have paired BOLD measurement with additional physiological scans to monitor specific sub-components of the BOLD signal. As a case study, vascular impairment is a known feature of cognitive aging in healthy adults (Snyder et al., 2015), but the same neurovascular coupling factor (from neuronal activity to hemodynamic response) is still often assumed in both young and elderly people. During a cognitive task, measured BOLD responses in the frontal cortex were similar between younger (mean age 24) and older adults (mean age 64) (Gauthier et al., 2013), which could naively be interpreted as the same level of neuronal activity in each group.

However, the investigators also measured brain perfusion with arterial spin labeling (ASL) in the same session, and observed 5% reduced CBF response to hypercapnia in elderly people. Through quantification with the calibrated BOLD model, older adults were found to have 15% lower maximal BOLD response (M) compared to younger adults (Gauthier et al., 2013). These additional ASL-based findings suggest that a given BOLD response in elderly people might correspond to a larger change in neuronal activity than the same measured BOLD response in younger people. Reduced absolute CBF in elderly cohorts (age 60–78 years) was confirmed by separate dual-echo BOLD/ASL experiments compared to younger cohorts (24–33 years) (De Vis et al., 2015a). Through the general calibrated model, these BOLD/ASL experiments also revealed lower $CMRO_2$ in elderly cohorts, presenting both vascular and metabolic baseline differences that influence the BOLD signal. Auxiliary

physiological scans such as ASL or direct OEF imaging thus are needed to interpret BOLD responses when compared across cohorts with different vascular physiology.

Finally, even more nuanced understandings of BOLD signals are made available with quantitative CBF scans. Baseline CBF and the neurovascular coupling constant (between $CMRO_2$ and CBF) both directly affect the BOLD signal amplitude; and there is evidence that the coupling constant itself is sensitive to baseline CBF (Whittaker et al., 2016). In addition to the mean BOLD signal, the standard deviation is also reduced in some populations including elderly people, indicative of impaired hemodynamic range (Garrett et al., 2017). Using simultaneous BOLD/ASL scans, a recent study corrected for vascular effects (CVR, CBF) on the standard deviation of the BOLD signal. Even after this correction, older adults still had lower BOLD variability compared to younger adults (Garrett et al., 2017). With ancillary ASL scans, vascular effects can thus be decoupled, revealing neuronal-specific changes in BOLD signal and BOLD variability that are important biomarkers of aging and neurological disease.

Given this understanding of the BOLD biophysical models, investigators can follow the following principles: (1) Acknowledge that multiple physiological components can change in disease and contribute to BOLD signal differences between patients. (2) Because neurovascular coupling can change for various patient groups, e.g. in elderly versus young patients (D'Esposito et al., 2003), test for relative BOLD differences between groups. For instance, BOLD changes during multiple behaviour or breathing tasks are more informative than comparing patient BOLD responses to a single task or at baseline. (3) Whenever possible, inform the interpretation of the BOLD signal with separate measurements of baseline physiological quantities in the same imaging session, as detailed in Fig. 2.

*Considerations for use of **quantitative** BOLD models in patients*

The use of calibrated BOLD models that enable baseline OEF mapping provides the most complete information, but also complex errors in disease applications. Because these models were originally formulated for normal physiology, the use of additional BOLD observations for calibration is difficult when cerebral physiology, or interactions between the physiological parameters (e.g. CBV and CBF), are perturbed in disease. Furthermore, many neurological disorders such as tumours are thought to exhibit extremely heterogeneous values of OEF and $CMRO_2$. If the assumed CBF change (e.g., in the hyperoxia model) or assumed neurovascular coupling is spatially uniform, the calibrated BOLD model results will not capture the true physiological heterogeneity in the tumour.

Table 1 addresses the major assumptions of the calibrated BOLD model and the potential error that results if these assumptions are not met in disease settings. The assumed coupling between CBV and CBF is likely the most problematic because changes in this coupling are often regional in nature (Eastwood and Provenzale, 2003; Peca et al., 2013) and depends on disease stage (Leigh et al., 2017). Especially in conditions where CBV and CBF are decoupled (e.g. a lack of autoregulation), results of the calibrated BOLD model will not be interpretable. Other assumptions of iso-metabolism and arterial O_2 content may not be met in pathological conditions, but are expected to create global measurement bias that can be corrected, or reduced sensitivity that requires higher SNR in the acquisition. A major strength of the calibrated BOLD methods is that the underlying models can be easily adapted to non-ideal conditions, given prior information about the brain physiology. For instance, when the iso-metabolic assumption is not met, known changes in metabolism

Table 1
Measurement effects if the assumptions of the calibrated BOLD model are not met in disease conditions.

Assumption	Breakdown and Example Neurological Disorder	Resulting Error
CBF to CBV coupling	• **Elevated coupling ratio:** Tumours show elevated CBV that is disproportionate to the CBF increase. (Akella et al., 2004; Eastwood and Provenzale, 2003) • **Uncoupling:** In stroke penumbra and steno-occlusive disease, reduced CBF is compensated initially by vessel dilation and increased CBV (Leigh et al., 2017)	•Changes in coupling ratio will lead to measurement bias. For instance, **overestimation** of changes in $CMRO_2$ occurs if **increased coupling ratio** is not accounted for (Davis et al., 1998). 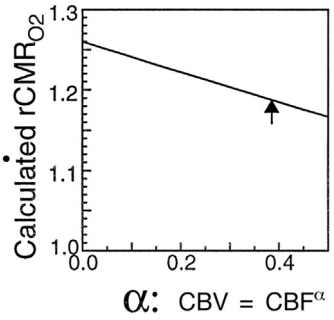 •When uncoupling is suspected, it is not appropriate to estimate CBV from the CBF response. Alternative CBV imaging strategies should be used with the model.
Iso-metabolism during mild CO_2 or O_2 inhalation	• Assumed iso-metabolism during gas challenges is debated even in healthy people, and may be more problematic in patients. •**Prolonged increases in $CMRO_2$** after hyperoxia treatment have been shown specifically in **tumour** tissue. (Rockswold et al., 2001; Rijpkema et al., 2002) •**Decreased $CMRO_2$** is observed with hyperoxia treatment for global ischemia after cardiac arrest, reflecting damage from oxidative molecular changes (Richards et al., 2007).	•If metabolism changes during the gas challenge, the resulting M parameter is not an appropriate calibration. •If **$CMRO_2$ increases** during gas breathing instead of remaining constant, the M parameter will be overestimated. This translates to **overestimation of $CMRO_2$ changes** during a separate functional task. •Calibrated BOLD methods that use multiple gas challenges will experience more complex interactions.
Arterial blood is fully saturated	•The calibrated BOLD models assume that arterial blood is fully oxygenated, but anemic or elderly/diabetic populations may have **lower arterial oxygenation.** •Similarly, the carrying capacity of oxygen is different for sickle cell populations with altered hemoglobin conformations.	•In the hyperoxia model, the relationship between measured end-tidal O_2 and the arterial content may not be accurate in patients •For quantification, CaO_2 (arterial O_2 content) is overestimated and leads to an **overestimation of oxygen extraction**

(e.g. from literature or other quantitative MRI scans) can be accounted for in Equations (2) and (3).

To select between different quantitative BOLD methods, investigators may first consider what is known a priori about neurovascular coupling in the specific disorder. If CBV and CBF changes are severely decoupled, or will change rapidly over the disease course, the calibrated BOLD model may not be appropriate. Instead, the investigators can consider adoption of more specific physiological imaging techniques, such as imaging CBV directly with VASO-based techniques instead of deriving CBV changes from ASL observations of perfusion. Vascular fingerprinting methods may also be a viable alternative if contrast is used for acquisition, enabling separation of CBV and oxygenation effects and a more flexible dictionary that accommodates disruptions to neurovascular coupling (Christen et al., 2014). Secondly, if OEF and $CMRO_2$ changes are spatially heterogeneous in the disease, investigators should avoid purely hyperoxic calibrations that assume a uniform CBF response. Instead, the investigators may prioritize carbogen and hypercapnic calibrations within an acquisition protocol that enables sufficient spatial resolution in the BOLD-ASL scan.

Conclusion

The BOLD signal is a valuable tool for detecting changes in neuronal activity in the human brain. While the BOLD signal is related to neuronal activity, the relationship between them is complex, involving a combination of changes in oxidative metabolism, blood flow and blood volume. Various models have been developed over the years to describe BOLD signal dynamics and its steady-state physiological component. One of the most useful BOLD signal models is the calibrated fMRI model. This model uses a hypercapnia manipulation to extract the vascular and metabolic components of this signal. Since its original description, this model has been extended to be valid for other breathing manipulations such as hyperoxia and carbogen breathing. More recent work has further extended the use of this model to measure baseline oxidative metabolism. The BOLD contrast and BOLD signal models can be used in the clinic to study tumours and cerebrovascular diseases. These quantitative models are especially useful for the understanding of cerebral diseases as they are more specific biomarkers of clinically-relevant physiological changes.

Acknowledgements

The authors would like to thank GE Healthcare, the Stanford Neuroscience Institute Interdisciplinary Scholar Award (A.P.F) and the Heart and Stroke Foundation of Canada for their financial support.

References

Aanerud, J., Borghammer, P., Chakravarty, M.M., Vang, K., Rodell, A.B., Jonsdottir, K.Y., Moller, A., Ashkanian, M., Vafaee, M.S., Iversen, P., Johannsen, P., Gjedde, A., 2012. Brain energy metabolism and blood flow differences in healthy aging. J. Cereb. Blood Flow. Metab. 32, 1177–1187.

Aaslid, R., Huber, P., Nornes, H., 1984. Evaluation of cerebrovascular spasm with transcranial Doppler ultrasound. J. Neurosurg. 60, 37–41.

Akella, Shastry, N., Twieg, Donald B., Mikkelsen, Tom, Hochberg, Fred H., Grossman, Stuart, Cloud, Gretchen A., Burt Nabors, L., 2004. Assessment of brain tumor angiogenesis inhibitors using perfusion magnetic resonance imaging: quality and analysis results of a phase I trial. J.Magn. Reson. Imag. 20 (6), 913–922.

An, H., Lin, W., 2000. Quantitative measurements of cerebral blood oxygen saturation using magnetic resonance imaging. J. Cereb. Blood Flow. Metab. 20, 1225–1236.

An, H., Lin, W., Celik, A., Lee, Y.Z., 2001. Quantitative measurements of cerebral metabolic rate of oxygen utilization using MRI: a volunteer study. NMR Biomed. 14, 441–447.

Ances, B., Vaida, F., Ellis, R., Buxton, R., 2011. Test-retest stability of calibrated BOLD-fMRI in HIV- and HIV+ subjects. Neuroimage 54, 2156–2162.

Ances, B.M., Leontiev, O., Perthen, J.E., Liang, C., Lansing, A.E., Buxton, R.B., 2008. Regional differences in the coupling of cerebral blood flow and oxygen metabolism changes in response to activation: implications for BOLD-fMRI. Neuroimage 39, 1510–1521.

Ances, B.M., Liang, C.L., Leontiev, O., Perthen, J.E., Fleisher, A.S., Lansing, A.E., Buxton, R.B., 2009. Effects of aging on cerebral blood flow, oxygen metabolism, and blood oxygenation level dependent responses to visual stimulation. Hum. Brain Mapp. 30, 1120–1132.

Aubert, A., Costalat, R., 2002. A model of the coupling between brain electrical activity, metabolism, and hemodynamics: application to the interpretation of functional neuroimaging. Neuroimage 17, 1162–1181.

Aubert, A., Pellerin, L., Magistretti, P.J., Costalat, R., 2007. A coherent neurobiological framework for functional neuroimaging provided by a model integrating compartmentalized energy metabolism. Proc. Natl. Acad. Sci. U. S. A. 104, 4188–4193.

Bartolo, M.J., Gieselmann, M.A., Vuksanovic, V., Hunter, D., Sun, L., Chen, X., Delicato, L.S., Thiele, A., 2011. Stimulus-induced dissociation of neuronal firing rates and local field potential gamma power and its relationship to the resonance blood oxygen level-dependent signal in macaque primary visual cortex. Eur. J. Neurosci. 34, 1857–1870.

Baudelet, C., Gallez, B., 2002. How does blood oxygen level-dependent (BOLD) contrast correlate with oxygen partial pressure (pO2) inside tumors? Magn. Reson Med. 48, 980–986.

Ben Bashat, D., Artzi, M., Ben Ami, H., Aizenstein, O., Blumenthal, D.T., Bokstein, F., Corn, B.W., Ram, Z., Kanner, A.A., Lifschitz-Mercer, B., Solar, I., Kolatt, T., Palmon, M., Edrei, Y., Abramovitch, R., 2012. Hemodynamic response imaging: a potential tool for the assessment of angiogenesis in brain tumors. PLoS One 7, e49416.

Bentley, W.J., Li, J.M., Snyder, A.Z., Raichle, M.E., Snyder, L.H., 2016. Oxygen level and LFP in task-positive and task-negative areas: bridging BOLD fMRI and electrophysiology. Cereb. Cortex 26, 346–357.

Bernardi, L., Gordin, D., Bordino, M., Rosengard-Barlund, M., Sandelin, A., Forsblom, C., Groop, P.H., 2017. Oxygen-induced impairment in arterial function is corrected by slow breathing in patients with type 1 diabetes. Sci. Rep. 7, 6001.

Berwick, J., Johnston, D., Jones, M., Martindale, J., Redgrave, P., McLoughlin, N., Mayhew, J.E.W., 2005. Neurovascular coupling investigated with two-dimensional optical imaging spectroscopy in rat whisker barrel cortex. Eur. J. Neurosci. 22, 1655–1666.

Blockley, N.P., Francis, S.T., Gowland, P.A., 2009. Perturbation of the BOLD response by a contrast agent and interpretation through a modified balloon model. Neuroimage 48, 84–93.

Blockley, N.P., Griffeth, V.E., Simon, A.B., Buxton, R.B., 2013. A review of calibrated blood oxygenation level-dependent (BOLD) methods for the measurement of task-induced changes in brain oxygen metabolism. NMR Biomed. 26, 987–1003.

Blockley, N.P., Griffeth, V.E., Stone, A.J., Hare, H.V., Bulte, D.P., 2015. Sources of systematic error in calibrated BOLD based mapping of baseline oxygen extraction fraction. Neuroimage 122, 105–113.

Blockley, N.P., Stone, A.J., 2016. Improving the specificity of R2' to the deoxyhaemoglobin content of brain tissue: prospective correction of macroscopic magnetic field gradients. Neuroimage 135, 253–260.

Bolar, D.S., Rosen, B.R., Sorensen, A.G., Adalsteinsson, E., 2011. QUantitative Imaging of eXtraction of oxygen and TIssue consumption (QUIXOTIC) using venular-targeted velocity-selective spin labeling. Magn. Reson Med. 66, 1550–1562.

Boxerman, J.L., Hamberg, L.M., Rosen, B.R., Weisskoff, R.M., 1995. MR contrast due to intravascular magnetic susceptibility perturbations. Magn. Reson Med. 34, 555–566.

Briers, J.D., 2001. Laser Doppler, speckle and related techniques for blood perfusion mapping and imaging. Physiol. Meas. 22, R35–R66.

Bulte, D.P., Drescher, K., Jezzard, P., 2009. Comparison of hypercapnia-based calibration techniques for measurement of cerebral oxygen metabolism with MRI. Magn. Reson Med. 61, 391–398.

Bulte, D.P., Kelly, M., Germuska, M., Xie, J., Chappell, M.A., Okell, T.W., Bright, M.G., Jezzard, P., 2012. Quantitative measurement of cerebral physiology using respiratory-calibrated MRI. Neuroimage 60, 582–591.

Buxton, R.B., 2010. Interpreting oxygenation-based neuroimaging signals: the importance and the challenge of understanding brain oxygen metabolism. Front. Neuroenergetics 2, 8.

Buxton, R.B., 2012. Dynamic models of BOLD contrast. Neuroimage 62, 953–961.

Buxton, R.B., Uludag, K., Dubowitz, D.J., Liu, T.T., 2004. Modeling the hemodynamic response to brain activation. Neuroimage 23 (Suppl 1), S220–S233.

Buxton, R.B., Wong, E.C., Frank, L.R., 1998. Dynamics of blood flow and oxygenation changes during brain activation: the balloon model. Magn. Reson Med. 39, 855–864.

Chen, J.J., Pike, G.B., 2009a. BOLD-specific cerebral blood volume and blood flow changes during neuronal activation in humans. NMR Biomed. 22, 1054–1062.

Chen, J.J., Pike, G.B., 2009b. Origins of the BOLD post-stimulus undershoot. Neuroimage 46, 559–568.

Chen, J.J., Pike, G.B., 2010. MRI measurement of the BOLD-specific flow-volume relationship during hypercapnia and hypocapnia in humans. Neuroimage 53, 383–391.

Cheng, Y.C., Haacke, E.M., 2001. Predicting BOLD signal changes as a function of blood volume fraction and resolution. NMR Biomed. 14, 468–477.

Chiarelli, P.A., Bulte, D.P., Wise, R., Gallichan, D., Jezzard, P., 2007. A calibration method for quantitative BOLD fMRI based on hyperoxia. Neuroimage 37, 808–820.

Christen, T., Bolar, D.S., Zaharchuk, G., 2013. Imaging brain oxygenation with MRI using blood oxygenation approaches: methods, validation, and clinical applications. AJNR Am. J. Neuroradiol. 34, 1113–1123.

Christen, T., Pannetier, N.A., Ni, W.W., Qiu, D., Moseley, M.E., Schuff, N., Zaharchuk, G., 2014. MR vascular fingerprinting: a new approach to compute cerebral blood volume, mean vessel radius, and oxygenation maps in the human brain. Neuroimage 89, 262–270.

Christen, T., Schmiedeskamp, H., Straka, M., Bammer, R., Zaharchuk, G., 2012. Measuring brain oxygenation in humans using a multiparametric quantitative blood oxygenation level dependent MRI approach. Magn. Reson Med. 68, 905–911.

Cohen, E.R., Rostrup, E., Sidaros, K., Lund, T.E., Paulson, O.B., Ugurbil, K., Kim, S.G., 2004. Hypercapnic normalization of BOLD fMRI: comparison across field strengths and pulse sequences. Neuroimage 23, 613–624.
D'Esposito, M., Deouell, L.Y., Gazzaley, A., 2003. Alterations in the BOLD fMRI signal with ageing and disease: a challenge for neuroimaging. Nat. Rev. Neurosci. 4, 863–872.
Davis, T.L., Kwong, K.K., Weisskoff, R.M., Rosen, B.R., 1998. Calibrated functional MRI: mapping the dynamics of oxidative metabolism. Proc. Natl. Acad. Sci. U. S. A. 95, 1834–1839.
De Vis, J.B., Hendrikse, J., Bhogal, A., Adams, A., Kappelle, L.J., Petersen, E.T., 2015a. Age-related changes in brain hemodynamics; A calibrated MRI study. Hum. Brain Mapp. 36, 3973–3987.
De Vis, J.B., Petersen, E.T., Bhogal, A., Hartkamp, N.S., Klijn, C.J., Kappelle, L.J., Hendrikse, J., 2015b. Calibrated MRI to evaluate cerebral hemodynamics in patients with an internal carotid artery occlusion. J. Cereb. Blood Flow. Metab. 35, 1015–1023.
Devor, A., Dunn, A.K., Andermann, M.L., Ulbert, I., Boas, D.A., Dale, A.M., 2003. Coupling of total hemoglobin concentration, oxygenation, and neural activity in rat somatosensory cortex. Neuron 39, 353–359.
Devor, A., Sakadzic, S., Saisan, P.A., Yaseen, M.A., Roussakis, E., Srinivasan, V.J., Vinogradov, S.A., Rosen, B.R., Buxton, R.B., Dale, A.M., Boas, D.A., 2011. "Overshoot" of O is required to maintain baseline tissue oxygenation at locations distal to blood vessels. J. Neurosci. 31, 13676–13681.
Donahue, M.J., Lu, H., Jones, C.K., Edden, R.A., Pekar, J.J., van Zijl, P.C., 2006. Theoretical and experimental investigation of the VASO contrast mechanism. Magn. Reson Med. 56, 1261–1273.
Donahue, M.J., Stevens, R.D., de Boorder, M., Pekar, J.J., Hendrikse, J., van Zijl, P.C., 2009. Hemodynamic changes after visual stimulation and breath holding provide evidence for an uncoupling of cerebral blood flow and volume from oxygen metabolism. J. Cereb. Blood Flow. Metab. 29, 176–185.
Dunn, J.F., O'Hara, J.A., Zaim-Wadghiri, Y., Lei, H., Meyerand, M.E., Grinberg, O.Y., Hou, H., Hoopes, P.J., Demidenko, E., Swartz, H.M., 2002. Changes in oxygenation of intracranial tumors with carbogen: a BOLD MRI and EPR oximetry study. J. Magn. Reson Imaging 16, 511–521.
Eastwood, J.D., Provenzale, J.M., 2003. Cerebral blood flow, blood volume, and vascular permeability of cerebral glioma assessed with dynamic CT perfusion imaging. Neuroradiology 45 (6), 373–376.
Eichling, J.O., Raichle, M.E., Grubb Jr., R.L., Larson, K.B., Ter-Pogossian, M.M., 1975. In vivo determination of cerebral blood volume with radioactive oxygen-15 in the monkey. Circ. Res. 37, 707–714.
Fan, A.P., Benner, T., Bolar, D.S., Rosen, B.R., Adalsteinsson, E., 2011. Phase-based regional oxygen metabolism (PROM) using MRI. Magn. Reson Med.
Fan, A.P., Schafer, A., Huber, L., Lampe, L., von Smuda, S., Moller, H.E., Villringer, A., Gauthier, C.J., 2016. Baseline oxygenation in the brain: correlation between respiratory-calibration and susceptibility methods. Neuroimage 125, 920–931.
Feng, C.M., Liu, H.L., Fox, P.T., Gao, J.H., 2001. Comparison of the experimental BOLD signal change in event-related fMRI with the balloon model. NMR Biomed. 14, 397–401.
Fox, P.T., Raichle, M.E., 1986. Focal physiological uncoupling of cerebral blood flow and oxidative metabolism during somatosensory stimulation in human subjects. Proc. Natl. Acad. Sci. U. S. A. 83, 1140–1144.
Francis, S.T., Pears, J.A., Butterworth, S., Bowtell, R.W., Gowland, P.A., 2003. Measuring the change in CBV upon cortical activation with high temporal resolution using look-locker EPI and Gd-DTPA. Magn. Reson Med. 50, 483–492.
Gagnon, L., Sakadzic, S., Lesage, F., Musacchia, J.J., Lefebvre, J., Fang, Q., Yucel, M.A., Evans, K.C., Mandeville, E.T., Cohen-Adad, J., Polimeni, J.R., Yaseen, M.A., Lo, E.H., Greve, D.N., Buxton, R.B., Dale, A.M., Devor, A., Boas, D.A., 2015. Quantifying the microvascular origin of BOLD-fMRI from first principles with two-photon microscopy and an oxygen-sensitive nanoprobe. J. Neurosci. 35, 3663–3675.
Gagnon, L., Sakadzic, S., Lesage, F., Pouliot, P., Dale, A.M., Devor, A., Buxton, R.B., Boas, D.A., 2016. Validation and optimization of hypercapnic-calibrated fMRI from oxygen-sensitive two-photon microscopy. Philos. Trans. R. Soc. Lond B Biol. Sci. 371.
Garrett, D.D., Lindenberger, U., Hoge, R.D., Gauthier, C.J., 2017. Age differences in brain signal variability are robust to multiple vascular controls. Sci. Rep. 7, 10149.
Gauthier, C.J., Desjardins-Crépeau, L., Madjar, C., Bherer, L., Hoge, R.D., 2012. Absolute quantification of resting oxygen metabolism and metabolic reactivity during functional activation using QUO2 MRI. Neuroimage 63, 1353–1363.
Gauthier, C.J., Hoge, R.D., 2012a. A generalized procedure for calibrated MRI incorporating hyperoxia and hypercapnia. Hum. Brain Mapp. 34, 1053–1069.
Gauthier, C.J., Hoge, R.D., 2012b. Magnetic resonance imaging of resting OEF and CMRO2 using a generalized calibration model for hypercapnia and hyperoxia. Neuroimage 60, 1212–1225.
Gauthier, C.J., Madjar, C., Desjardins-Crepeau, L., Bellec, P., Bherer, L., Hoge, R.D., 2013. Age dependence of hemodynamic response characteristics in human functional magnetic resonance imaging. Neurobiol. Aging 34, 1469–1485.
Gauthier, C.J., Madjar, C., Tancredi, F.B., Stefanovic, B., Hoge, R.D., 2011. Elimination of visually evoked BOLD responses during carbogen inhalation: implications for calibrated MRI. Neuroimage 54, 1001–1011.
Geranmayeh, F., Wise, R.J., Leech, R., Murphy, K., 2015. Measuring vascular reactivity with breath-holds after stroke: a method to aid interpretation of group-level BOLD signal changes in longitudinal fMRI studies. Hum. Brain Mapp. 36, 1755–1771.
Germuska, M., Merola, A., Murphy, K., Babic, A., Richmond, L., Khot, S., Hall, J.E., Wise, R.G., 2016. A forward modelling approach for the estimation of oxygen extraction fraction by calibrated fMRI. Neuroimage 139, 313–323.
Girouard, H., Iadecola, C., 2006. Neurovascular coupling in the normal brain and in hypertension, stroke, and Alzheimer disease. J. Appl. Physiol. 100, 328–335.
Griffeth, V.E., Buxton, R.B., 2011. A theoretical framework for estimating cerebral oxygen metabolism changes using the calibrated-BOLD method: modeling the effects of blood volume distribution, hematocrit, oxygen extraction fraction, and tissue signal properties on the BOLD signal. Neuroimage 58, 198–212.
Hallac, R.R., Zhou, H., Pidikiti, R., Song, K., Stojadinovic, S., Zhao, D., Solberg, T., Peschke, P., Mason, R.P., 2014. Correlations of noninvasive BOLD and TOLD MRI with pO2 and relevance to tumor radiation response. Magn. Reson Med. 71, 1863–1873.
Hare, H.V., Blockley, N.P., Gardener, A.G., Clare, S., Bulte, D.P., 2015. Investigating the field-dependence of the Davis model: calibrated fMRI at 1.5, 3 and 7T. Neuroimage 112, 189–196.
Hattori, N., Bergsneider, M., Wu, H.M., Glenn, T.C., Vespa, P.M., Hovda, D.A., Phelps, M.E., Huang, S.C., 2004. Accuracy of a method using short inhalation of (15) O-O(2) for measuring cerebral oxygen extraction fraction with PET in healthy humans. J. Nucl. Med. 45, 765–770.
Havlicek, M., Ivanov, D., Poser, B.A., Uludag, K., 2017a. Echo-time dependence of the BOLD response transients - a window into brain functional physiology. Neuroimage 159, 355–370.
Havlicek, M., Roebroeck, A., Friston, K., Gardumi, A., Ivanov, D., Uludag, K., 2015. Physiologically informed dynamic causal modeling of fMRI data. Neuroimage 122, 355–372.
Havlicek, M., Roebroeck, A., Friston, K.J., Gardumi, A., Ivanov, D., Uludag, K., 2017b. On the importance of modeling fMRI transients when estimating effective connectivity: a dynamic causal modeling study using ASL data. Neuroimage 155, 217–233.
He, X., Yablonskiy, D.A., 2007. Quantitative BOLD: mapping of human cerebral deoxygenated blood volume and oxygen extraction fraction: default state. Magn. Reson Med. 57, 115–126.
He, X., Zhu, M., Yablonskiy, D.A., 2008. Validation of oxygen extraction fraction measurement by qBOLD technique. Magn. Reson Med. 60, 882–888.
Hoge, R.D., Atkinson, J., Gill, B., Crelier, G.R., Marrett, S., Pike, G.B., 1999. Investigation of BOLD signal dependence on cerebral blood flow and oxygen consumption: the deoxyhemoglobin dilution model. Magn. Reson Med. 42, 849–863.
Hua, J., Stevens, R.D., Huang, A.J., Pekar, J.J., van Zijl, P.C., 2011. Physiological origin for the BOLD poststimulus undershoot in human brain: vascular compliance versus oxygen metabolism. J. Cereb. Blood Flow. Metab. 31, 1599–1611.
Huber, L., Ivanov, D., Handwerker, D.A., Marrett, S., Guidi, M., Uludag, K., Bandettini, P.A., Poser, B.A., 2018. Techniques for blood volume fMRI with VASO: from low-resolution mapping towards sub-millimeter layer-dependent applications. Neuroimage 164, 131–143.
Hutchison, J.L., Shokri-Kojori, E., Lu, H., Rypma, B., 2013. A BOLD perspective on age-related neurometabolic-flow coupling and neural efficiency changes in human visual cortex. Front. Psychol. 4, 244.
Hyder, F., Herman, P., Bailey, C.J., Moller, A., Globinsky, R., Fulbright, R.K., Rothman, D.L., Gjedde, A., 2016. Uniform distributions of glucose oxidation and oxygen extraction in gray matter of normal human brain: No evidence of regional differences of aerobic glycolysis. J. Cereb. Blood Flow. Metab. 36, 903–916.
Ibaraki, M., Miura, S., Shimosegawa, E., Sugawara, S., Mizuta, T., Ishikawa, A., Amano, M., 2008. Quantification of cerebral blood flow and oxygen metabolism with 3-dimensional PET and 15O: validation by comparison with 2-dimensional PET. J. Nucl. Med. 49, 50–59.
Ibaraki, M., Shinohara, Y., Nakamura, K., Miura, S., Kinoshita, F., Kinoshita, T., 2010. Interindividual variations of cerebral blood flow, oxygen delivery, and metabolism in relation to hemoglobin concentration measured by positron emission tomography in humans. J. Cereb. Blood Flow. Metab. 30, 1296–1305.
Ishii, K., Kitagaki, H., Kono, M., Mori, E., 1996a. Decreased medial temporal oxygen metabolism in Alzheimer's disease shown by PET. J. Nucl. Med. 37, 1159–1165.
Ishii, K., Sasaki, M., Kitagaki, H., Sakamoto, S., Yamaji, S., Maeda, K., 1996b. Regional difference in cerebral blood flow and oxidative metabolism in human cortex. J. Nucl. Med. 37, 1086–1088.
Ito, H., Ibaraki, M., Kanno, I., Fukuda, H., Miura, S., 2005. Changes in cerebral blood flow and cerebral oxygen metabolism during neural activation measured by positron emission tomography: comparison with blood oxygenation level-dependent contrast measured by functional magnetic resonance imaging. J. Cereb. Blood Flow. Metab. 25, 371–377.
Ito, H., Kanno, I., Kato, C., Sasaki, T., Ishii, K., Ouchi, Y., Iida, A., Okazawa, H., Hayashida, K., Tsuyuguchi, N., Kuwabara, Y., Senda, M., 2004. Database of normal human cerebral blood flow, cerebral blood volume, cerebral oxygen extraction fraction and cerebral metabolic rate of oxygen measured by positron emission tomography with 15O-labelled carbon dioxide or water, carbon monoxide and oxygen: a multicentre study in Japan. Eur. J. Nucl. Med. Mol. Imaging 31, 635–643.
Jain, V., Langham, M.C., Wehrli, F.W., 2010. MRI estimation of global brain oxygen consumption rate. J. Cereb. Blood Flow. Metab. 30, 1598–1607.
Jin, T., Kim, S.G., 2008. Improved cortical-layer specificity of vascular space occupancy fMRI with slab inversion relative to spin-echo BOLD at 9.4 T. Neuroimage 40, 59–67.
Kety, S.S., Schmidt, C.F., 1948. The effects of altered arterial tensions of carbon dioxide and oxygen on cerebral blood flow and cerebral oxygen consumption of normal young men. J. Clin. Invest. 27, 484–492.
Kilner, J.M., Mattout, J., Henson, R., Friston, K.J., 2005. Hemodynamic correlates of EEG: a heuristic. Neuroimage 28, 280–286.
Kim, S.G., Harel, N., Jin, T., Kim, T., Lee, P., Zhao, F., 2013. Cerebral blood volume MRI with intravascular superparamagnetic iron oxide nanoparticles. NMR Biomed. 26, 949–962.
Kong, Y., Zheng, Y., Johnston, D., Martindale, J., Jones, M., Billings, S., Mayhew, J., 2004. A model of the dynamic relationship between blood flow and volume changes during brain activation. J. Cereb. Blood Flow. Metab. 24, 1382–1392.

Krieger, S.N., Gauthier, C.J., Ivanov, D., Huber, L., Roggenhofer, E., Sehm, B., Turner, R., Egan, G.F., 2014. Regional reproducibility of calibrated BOLD functional MRI: implications for the study of cognition and plasticity. Neuroimage 101C, 8–20.
Lajoie, I., Tancredi, F.B., Hoge, R.D., 2016. Regional reproducibility of BOLD calibration parameter M, OEF and resting-state CMRO2 measurements with QUO2 MRI. PLoS One 11, e0163071.
Lauritzen, M., Gold, L., 2003. Brain function and neurophysiological correlates of signals used in functional neuroimaging. J. Neurosci. 23, 3972–3980.
Lecrux, C., Hamel, E., 2011. The neurovascular unit in brain function and disease. Acta Physiol. (Oxf) 203, 47–59.
Lecrux, C., Hamel, E., 2016. Neuronal networks and mediators of cortical neurovascular coupling responses in normal and altered brain states. Philos. Trans. R. Soc. Lond B Biol. Sci. 371.
Lee, S.P., Duong, T.Q., Yang, G., Iadecola, C., Kim, S.G., 2001. Relative changes of cerebral arterial and venous blood volumes during increased cerebral blood flow: implications for BOLD fMRI. Magn. Reson Med. 45, 791–800.
Leigh, R., Knutsson, L., Zhou, J., van Zijl, P.C., 2017. Imaging the physiological evolution of the ischemic penumbra in acute ischemic stroke. J. Cereb. Blood Flow. Metab. 271678X17700913.
Leontiev, O., Buracas, G.T., Liang, C., Ances, B.M., Perthen, J.E., Shmuel, A., Buxton, R.B., 2013. Coupling of cerebral blood flow and oxygen metabolism is conserved for chromatic and luminance stimuli in human visual cortex. Neuroimage 68, 221–228.
Leontiev, O., Buxton, R.B., 2007. Reproducibility of BOLD, perfusion, and CMRO2 measurements with calibrated-BOLD fMRI. Neuroimage 35, 175–184.
Levy, D.E., Brierley, J.B., Silverman, D.G., Plum, F., 1975. Brief hypoxia-ischemia initially damages cerebral neurons. Arch. Neurol. 32, 450–456.
Liu, P., Hebrank, A.C., Rodrigue, K.M., Kennedy, K.M., Section, J., Park, D.C., Lu, H., 2013. Age-related differences in memory-encoding fMRI responses after accounting for decline in vascular reactivity. Neuroimage 78, 415–425.
Liu, T.T., 2013. Neurovascular factors in resting-state functional MRI. Neuroimage 80, 339–348.
Logothetis, N.K., Pauls, J., Augath, M., Trinath, T., Oeltermann, A., 2001. Neurophysiological investigation of the basis of the fMRI signal. Nature 412, 150–157.
Logothetis, N.K., Wandell, B.A., 2004. Interpreting the BOLD signal. Annu. Rev. Physiol. 66, 735–769.
Lu, H., Donahue, M.J., van Zijl, P.C., 2006. Detrimental effects of BOLD signal in arterial spin labeling fMRI at high field strength. Magn. Reson Med. 56, 546–552.
Lu, H., Ge, Y., 2008. Quantitative evaluation of oxygenation in venous vessels using T2-Relaxation-Under-Spin-Tagging MRI. Magn. Reson Med. 60, 357–363.
Lu, H., van Zijl, P.C., 2012. A review of the development of Vascular-Space-Occupancy (VASO) fMRI. Neuroimage.
Lu, H., Xu, F., Grgac, K., Liu, P., Qin, Q., van Zijl, P., 2012. Calibration and validation of TRUST MRI for the estimation of cerebral blood oxygenation. Magn. Reson Med. 67, 42–49.
Lu, H., Xu, F., Rodrigue, K.M., Kennedy, K.M., Cheng, Y., Flicker, B., Hebrank, A.C., Uh, J., Park, D.C., 2011. Alterations in cerebral metabolic rate and blood supply across the adult lifespan. Cereb. Cortex 21, 1426–1434.
Magri, C., Schridde, U., Murayama, Y., Panzeri, S., Logothetis, N.K., 2012. The amplitude and timing of the BOLD signal reflects the relationship between local field potential power at different frequencies. J. Neurosci. 32, 1395–1407.
Malonek, D., Dirnagl, U., Lindauer, U., Yamada, K., Kanno, I., Grinvald, A., 1997. Vascular imprints of neuronal activity: relationships between the dynamics of cortical blood flow, oxygenation, and volume changes following sensory stimulation. Proc. Natl. Acad. Sci. U. S. A. 94, 14826–14831.
Mandell, D.M., Han, J.S., Poublanc, J., Crawley, A.P., Stainsby, J.A., Fisher, J.A., Mikulis, D.J., 2008. Mapping cerebrovascular reactivity using blood oxygen level-dependent MRI in Patients with arterial steno-occlusive disease: comparison with arterial spin labeling MRI. Stroke 39, 2021–2028.
Mandeville, J.B., Marota, J.J., Ayata, C., Zaharchuk, G., Moskowitz, M.A., Rosen, B.R., Weisskoff, R.M., 1999. Evidence of a cerebrovascular postarteriole windkessel with delayed compliance. J. Cereb. Blood Flow. Metab. 19, 679–689.
Mark, C.I., Fisher, J.A., Pike, G.B., 2011. Improved fMRI calibration: precisely controlled hyperoxic versus hypercapnic stimuli. Neuroimage 54, 1102–1111.
Merola, A., Murphy, K., Stone, A.J., Germuska, M.A., Griffeth, V.E., Blockley, N.P., Buxton, R.B., Wise, R.G., 2016. Measurement of oxygen extraction fraction (OEF): An optimized BOLD signal model for use with hypercapnic and hyperoxic calibration. Neuroimage 129, 159–174.
Mintun, M.A., Vlassenko, A.G., Shulman, G.L., Snyder, A.Z., 2002. Time-related increase of oxygen utilization in continuously activated human visual cortex. Neuroimage 16, 531–537.
Mohtasib, R.S., Lumley, G., Goodwin, J.A., Emsley, H.C., Sluming, V., Parkes, L.M., 2012. Calibrated fMRI during a cognitive Stroop task reveals reduced metabolic response with increasing age. Neuroimage 59, 1143–1151.
Nagata, K., Maruya, H., Yuya, H., Terashi, H., Mito, Y., Kato, H., Sato, M., Satoh, Y., Watahiki, Y., Hirata, Y., Yokoyama, E., Hatazawa, J., 2000. Can PET data differentiate Alzheimer's disease from vascular dementia? Ann. N. Y. Acad. Sci. 903, 252–261.
Ni, W., Christen, T., Zun, Z., Zaharchuk, G., 2015. Comparison of R2' measurement methods in the normal brain at 3 Tesla. Magn. Reson Med. 73, 1228–1236.
Ogawa, S., Lee, T.M., Kay, A.R., Tank, D.W., 1990a. Brain magnetic resonance imaging with contrast dependent on blood oxygenation. Proc. Natl. Acad. Sci. U. S. A. 87, 9868–9872.
Ogawa, S., Lee, T.M., Nayak, A.S., Glynn, P., 1990b. Oxygenation-sensitive contrast in magnetic resonance image of rodent brain at high magnetic fields. Magn. Reson Med. 14, 68–78.
Ogburn-Russell, L., Johnson, J.E., 1990. Oxygen saturation levels in the well elderly: altitude makes a difference. J. Gerontol. Nurs. 16, 26–30.
Peca, S., McCreary, C.R., Donaldson, E., Kumarpillai, G., Shobha, N., Sanchez, K., Charlton, A., Steinback, C.D., Beaudin, A.E., Fluck, D., Pillay, N., Fick, G.H., Poulin, M.J., Frayne, R., Goodyear, B.G., Smith, E.E., 2013. Neurovascular decoupling is associated with severity of cerebral amyloid angiopathy. Neurology 81, 1659–1665.
Peng, S.L., Dumas, J.A., Park, D.C., Liu, P., Filbey, F.M., McAdams, C.J., Pinkham, A.E., Adinoff, B., Zhang, R., Lu, H., 2014. Age-related increase of resting metabolic rate in the human brain. Neuroimage 98, 176–183.
Perthen, J.E., Lansing, A.E., Liau, J., Liu, T.T., Buxton, R.B., 2008. Caffeine-induced uncoupling of cerebral blood flow and oxygen metabolism: a calibrated BOLD fMRI study. Neuroimage 40, 237–247.
Pike, G.B., 2012. Quantitative functional MRI: concepts, issues and future challenges. Neuroimage 62, 1234–1240.
Pouliot, P., Gagnon, L., Lam, T., Avti, P.K., Bowen, C., Desjardins, M., Kakkar, A.K., Thorin, E., Sakadzic, S., Boas, D.A., Lesage, F., 2017. Magnetic resonance fingerprinting based on realistic vasculature in mice. Neuroimage 149, 436–445.
Richards, Erica M., Fiskum, Gary, Rosenthal, Robert E., Hopkins, Irene, McKenna, Mary C., 2007. Hyperoxic reperfusion after global ischemia decreases hippocampal energy metabolism. Stroke 38 (5), 1578–1584.
Rijpkema, Mark, Kaanders, Johannes HAM., Joosten, Frank BM., van der Kogel, Albert J., Heerschap, Arend, 2002. Effects of breathing a hyperoxic hypercapnic gas mixture on blood oxygenation and vascularity of head-and-neck tumors as measured by magnetic resonance imaging. Int. J. Radiat. Oncol. Biol. Phys. 53 (5), 1185–1191.
Rockswold, Sarah B., Rockswold, Gaylan L., Vargo, Janet M., Erickson, Carla A., Sutton, Richard L., Bergman, Thomas A., Biros, Michelle H., March 2001. Effects of hyperbaric oxygenation therapy on cerebral metabolism and intracranial pressure in severely brain injured patients. J. Neurosurg. 94 (3), 403–411.
Rodgers, Z.B., Detre, J.A., Wehrli, F.W., 2016. MRI-based methods for quantification of the cerebral metabolic rate of oxygen. J. Cereb. Blood Flow. Metab. 36, 1165–1185.
Seifritz, E., Bilecen, D., Hanggi, D., Haselhorst, R., Radu, E.W., Wetzel, S., Seelig, J., Scheffler, K., 2000. Effect of ethanol on BOLD response to acoustic stimulation: implications for neuropharmacological fMRI. Psychiatry Res. 99, 1–13.
Shmuel, A., Yacoub, E., Pfeuffer, J., Van de Moortele, P.F., Adriany, G., Hu, X., Ugurbil, K., 2002. Sustained negative BOLD, blood flow and oxygen consumption response and its coupling to the positive response in the human brain. Neuron 36, 1195–1210.
Snyder, H.M., Corriveau, R.A., Craft, S., Faber, J.E., Greenberg, S.M., Knopman, D., Lamb, B.T., Montine, T.J., Nedergaard, M., Schaffer, C.B., Schneider, J.A., Wellington, C., Wilcock, D.M., Zipfel, G.J., Zlokovic, B., Bain, L.J., Bosetti, F., Galis, Z.S., Koroshetz, W., Carrillo, M.C., 2015. Vascular contributions to cognitive impairment and dementia including Alzheimer's disease. Alzheimers Dement. 11, 710–717.
Stefanovic, B., Pike, G.B., 2005. Venous refocusing for volume estimation: VERVE functional magnetic resonance imaging. Magn. Reson Med. 53, 339–347.
Stone, A.J., Blockley, N.P., 2017. A streamlined acquisition for mapping baseline brain oxygenation using quantitative BOLD. Neuroimage 147, 79–88.
Suri, S., Mackay, C.E., Kelly, M.E., Germuska, M., Tunbridge, E.M., Frisoni, G.B., Matthews, P.M., Ebmeier, K.P., Bulte, D.P., Filippini, N., 2014. Reduced cerebrovascular reactivity in young adults carrying the APOE epsilon4 allele. Alzheimers Dement.
Taylor, N.J., Baddeley, H., Goodchild, K.A., Powell, M.E., Thoumine, M., Culver, L.A., Stirling, J.J., Saunders, M.I., Hoskin, P.J., Phillips, H., Padhani, A.R., Griffiths, J.R., 2001. BOLD MRI of human tumor oxygenation during carbogen breathing. J. Magn. Reson Imaging 14, 156–163.
Toronov, V., Walker, S., Gupta, R., Choi, J.H., Gratton, E., Hueber, D., Webb, A., 2003. The roles of changes in deoxyhemoglobin concentration and regional cerebral blood volume in the fMRI BOLD signal. Neuroimage 19, 1521–1531.
Uludag, K., Muller-Bierl, B., Ugurbil, K., 2009. An integrative model for neuronal activity-induced signal changes for gradient and spin echo functional imaging. Neuroimage 48, 150–165.
van Zijl, P.C., Eleff, S.M., Ulatowski, J.A., Oja, J.M., Ulug, A.M., Traystman, R.J., Kauppinen, R.A., 1998. Quantitative assessment of blood flow, blood volume and blood oxygenation effects in functional magnetic resonance imaging. Nat. Med. 4, 159–167.
van Zijl, P.C., Hua, J., Lu, H., 2012. The BOLD post-stimulus undershoot, one of the most debated issues in fMRI. Neuroimage 62, 1092–1102.
Vazquez, A.L., Fukuda, M., Tasker, M.L., Masamoto, K., Kim, S.G., 2010. Changes in cerebral arterial, tissue and venous oxygenation with evoked neural stimulation: implications for hemoglobin-based functional neuroimaging. J. Cereb. Blood Flow. Metab. 30, 428–439.
Vold, M.L., Aasebo, U., Melbye, H., 2014. Low FEV1, smoking history, and obesity are factors associated with oxygen saturation decrease in an adult population cohort. Int. J. Chron. Obstruct Pulmon Dis. 9, 1225–1233.
Wehrli, F.W., Fan, A.P., Rodgers, Z.B., Englund, E.K., Langham, M.C., 2016. Susceptibility-based time-resolved whole-organ and regional tissue oximetry. NMR Biomed.
Whittaker, J.R., Driver, I.D., Bright, M.G., Murphy, K., 2016. The absolute CBF response to activation is preserved during elevated perfusion: implications for neurovascular coupling measures. Neuroimage 125, 198–207.
Wise, R.G., Harris, A.D., Stone, A.J., Murphy, K., 2013. Measurement of OEF and absolute CMRO: MRI-based methods using interleaved and combined hypercapnia and hyperoxia. Neuroimage 83C, 135–147.
Xu, F., Liu, P., Lu, H., 2011a. Effect of graded O2 challenge on vascular and metabolic parameters. Proc. Intl. Soc. Mag. Reson. Med. 19th annual meeting, 765.

Xu, F., Uh, J., Brier, M.R., Hart Jr., J., Yezhuvath, U.S., Gu, H., Yang, Y., Lu, H., 2011b. The influence of carbon dioxide on brain activity and metabolism in conscious humans. J. Cereb. Blood Flow. Metab. 31, 58–67.
Yablonskiy, D.A., Haacke, E.M., 1994. Theory of NMR signal behavior in magnetically inhomogeneous tissues: the static dephasing regime. Magn. Reson Med. 32, 749–763.
Yablonskiy, D.A., Haacke, E.M., 1997. An MRI method for measuring T2 in the presence of static and RF magnetic field inhomogeneities. Magn. Reson Med. 37, 872–876.
Yamaguchi, T., Kanno, I., Uemura, K., Shishido, F., Inugami, A., Ogawa, T., Murakami, M., Suzuki, K., 1986. Reduction in regional cerebral metabolic rate of oxygen during human aging. Stroke 17, 1220–1228.
Yamauchi, H., Nishii, R., Higashi, T., Kagawa, S., Fukuyama, H., 2009. Hemodynamic compromise as a cause of internal border-zone infarction and cortical neuronal damage in atherosclerotic middle cerebral artery disease. Stroke 40, 3730–3735.
Yamauchi, H., Okazawa, H., Kishibe, Y., Sugimoto, K., Takahashi, M., 2002. Changes in blood flow and oxygen metabolism during visual stimulation in carotid artery disease: effect of baseline perfusion and oxygen metabolism. Stroke 33, 1294–1300.
Zappe, A.C., Uludag, K., Oeltermann, A., Ugurbil, K., Logothetis, N.K., 2008. The influence of moderate hypercapnia on neural activity in the anesthetized nonhuman primate. Cereb. Cortex 18, 2666–2673.
Zhang, J., Zhou, D., Nguyen, T.D., Spincemaille, P., Gupta, A., Wang, Y., 2016. Cerebral metabolic rate of oxygen (CMRO2) mapping with hyperventilation challenge using quantitative susceptibility mapping (QSM). Magn. Reson Med.
Zheng, Y., Mayhew, J., 2009. A time-invariant visco-elastic windkessel model relating blood flow and blood volume. Neuroimage 47, 1371–1380.